Dynamically Balanced Trajectory Generation for Non-Holonomic Forklift Vehicles

Leng Vongchanh, Alireza Mohammadi, Allison Kealy, Denny Oetomo
University of Melbourne, Australia
blv@student.unimelb.edu.au

Abstract

This paper proposes a trajectory planner for a non-holonomic wheeled mobile manipulator, specifically designed for a forklift vehicle (FLV). The planner addresses the high risk toppling, in both the lateral and sagittal directions, by integrating dynamic balance of the system in the design of the trajectory. The proposed trajectory extends the Dubins' and simple continuous curvature (SCC) paths, using time dependent parameters to build the path, while the dynamic balance is considered through the use of the zero moment point (ZMP) and a barycentric coordinate system to develop a scalar measure of toppling propensity. This geometric form was chosen to reduce the problem search space in consideration for industrial application. An computational illustration will compare existing paths and highlight the benefits for use with an FLV.

Figure 1: R1.4 Hyster Reach Truck, an example of a common FLV.

1 Introduction

Forklift vehicles (FLVs) are materials handling vehicles commonly used worldwide. An example of an FLV is shown in Figure 1. FLVs are not subject to safety standards used in automotive vehicles, for example safety interlocks, a logically conditioned seatbelt check, are not standard. Safety is addressed by requiring operator training for ridable FLVs, where training may be as short as two days. The lack of required safety measures is reflected by the Victorian WorkCover Authority [2012], reporting 250 serious injuries per year in Victoria. Larsson and Rechnitzer [1994] concluded that as FLVs are not categorised as a vehicle, they are not subject to systematic traffic management in the workplace.

There are two main safety issues that need to be addressed: collisions due to obstructed view caused by the load, and unbalancing of the vehicle in the lateral direction (roll over) or sagittal direction (tip over). For brevity, this paper will use the term toppling to describe loss of balance in either direction. FLVs generally carry the load in the forward direction of travel, with large loads obstructing forward view. The former problem is typically solved by the separation of the environment [Horberry *et al.*, 2004]; however this is less effective in picking/packing areas or aisles, where close proximity to structures or pedestrians is required. The latter problem is due to the construction of the vehicle, where the FLV may become unbalanced. This is a result of the compromise between versatility and safety. Driving training is used to reduce the likelihood of this type of accident; however the task of driving is typically repetitive and subject to operator fatigue.

This paper will focus mainly on the second problem of toppling by way of automation. Literature regarding automated storage and retrieval systems (AS/RS) focus on the modelling for efficiency [Gagliardi *et al.*,

2012]. Other systems, including the commercial KIVA system, are operated with velocities and accelerations such that the dynamic balance need not be considered. Many studies in the space of robotic automation often do not consider the issue of robot toppling, while studies on dynamic balance generally conclude on models that may be used to further study the desired vehicle without use in an automated setting [Popescu and Nastase, 2012].

To address the issue of toppling, the dynamic balance of the system must be considered. A mechanical system may be described as dynamically balanced if the system is not in an uncontrolled fall [Vukobratović *et al.*, 2006]. The zero moment point (ZMP), developed in the study of robotic gait, is one useful tool in determining the dynamic balance [Vukobratović and Juricic, 1969]. The ZMP, typically used for robotic gait synthesis [Vukobratović and Borovac, 2004], has more recently been used in mobile manipulators and automotive vehicles. Lapapong and Brennan [2010] introduce vehicle roll on banked turns using the ZMP, extending the ZMP for changing orientation planar surfaces. More closely related to FLVs, study on agricultural vehicles with forklift attachments consider, again, the slope of the environment [Popescu and Nastase, 2012].

In this paper, we aim to achieve autonomous operation of a FLV through the tracking of a planned trajectory that takes into account the dynamic balance of the FLV.

The ZMP provides the location of a point within the support polygon (SP) where the net moment of the system in motion is zero. To allow incorporation into the trajectory planning procedures, the measure of dynamic balance must be expressed as an inequality. The dynamic balance margin, previously coined as stability margin, is a scalar value that measures the balance. In this paper we use the term dynamic balance margin to differentiate between the stability in the control sense, similar to the differentiation of stability and dynamic balance defined by Vukobratović [2006]. This paper will propose a dynamic balance margin utilising the ZMP for an FLV.

Girbés, et al [2014] considers dynamic balance for a hybrid controller in automated guided vehicles (AGV), in this case an automated FLV. Double continuous curvature (DCC) paths are used to allow non-holonomic tracking of an unknown path using a set distance look-ahead. The controller uses two one-dimensional functions to describe the dynamic balance; however this ignores some of the coupling between states affecting balance. The proposed dynamic balance margin will consider a single two-dimensional problem that considers the coupled behaviour in more detail.

The DCC path is similar to another path known as simple continuous curvature (SCC) paths [Scheuer and Fraichard, 1997]. The SCC path is a geometrically planned path with continuous curvature, or G^2 geometric continuity, designed for use in non-holonomic paths given known terminal poses. The SCC path is based on the optimal distance Dubins' path. The enforcement of G^2 continuity, over the Dubin's path's G^1 continuity, results in sub-optimal distance; however, retains the benefit of easy computation. The SCC path, however, does not consider time changing parameters resulting in a highly conservative path.

In this paper, the proposed dynamic balance margin is incorporated into the selected C^2 continuous trajectory planning technique. It is therefore necessary to introduce the element of time into these geometric paths, such that the dynamic balance margin can be achieved. The trajectory planning method proposed here are based on the SCC path introduced above and labelled here as Modified SCC path.

The remainder of this paper will be organised as follows. The dynamic model used in this paper will be described in Section 2 and will go on to describe the ZMP. We propose a dynamic balance margin to be used in Section 3. The Dubins' and SCC paths will be briefly presented in Section 4 with the proposed modifications, focusing on combining the dynamics described in previous sections, to be presented in Section 5. A computational illustration and comparison will be discussed in Section 6. Section 7 will conclude the paper.

2 Dynamic model

The system will be modelled using a tricycle kinematic model shown in Figure 2, using the ZMP to describe the dynamic balance. The body frame x_1y_1 is centred at point O and can be used to describe the dimensions of the vehicle, the ZMP and centre of gravity (CoG). The radius of curvature $R = 1/\kappa = d/\tan\alpha$. The track t is the distance between the two passive wheels at point B and C, while the wheelbase d is the distance between O and the rear driven/steered wheel at point A.

This paper will not use the typical tricycle model where A is considered the front of the vehicle, but rather use point A as the rear. This model will be described by point O using the coordinates (x, y, θ). The linear velocity of the wheel $v_w = r_w\dot{\rho}$, where r_w is the radius of the wheel and $\dot{\rho}$ is the angular velocity of the wheel, and angular velocity of the steered wheel ω_α control the vehicle velocity and direction. The steering angle α will be used as the final state. The kinematics can be summarised as the following:

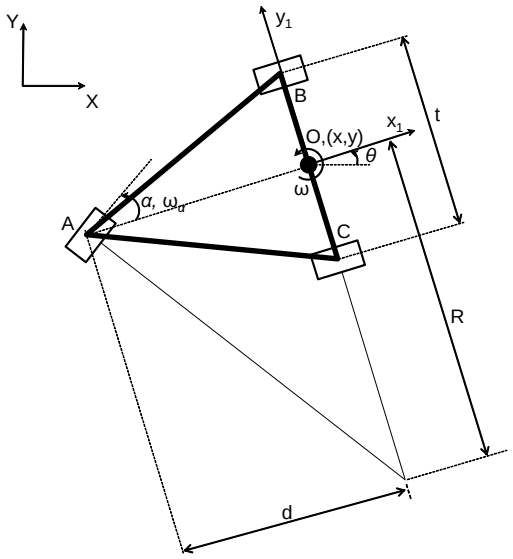

Figure 2: Kinematic model for 3 wheeled FLV. The geometry is defined by the wheelbase d and track t. The radius of curvature R may be calculated from the steering angle α.

$$\begin{bmatrix} \dot{X} \\ \dot{Y} \\ \dot{\theta} \\ \dot{\alpha} \end{bmatrix} = \begin{bmatrix} \sin\theta\cos\alpha & 0 \\ \cos\theta\cos\alpha & 0 \\ 1/R & 0 \\ 0 & 1 \end{bmatrix} \begin{bmatrix} v_w \\ \omega_\alpha \end{bmatrix} \tag{1}$$

Now that we have defined the kinematics, we may define the dynamic balance using the ZMP. The ZMP describes a point on the ground that corresponds to the zero moment of the system. If the ZMP lies within the support polygon (SP), the convex polygon ABC, then the system is dynamically balanced. The ZMP degenerates at the edge of the SP, where the ZMP no longer exists, corresponding to a dynamically unbalanced state. The ZMP can be calculated by measuring the ground reaction forces at the vertices of the SP, where the centre of action is the ZMP. This paper will use the d'Alembert formulation of the ZMP using the following equations:

$$y_{ZMP} = \frac{\sum_{i=1}^{n}(r_{i_y}m_i a_{i_z} - r_{i_z}m_i a_{i_y} + \dot{H}_{i_x}}{\sum_{i=1}^{n}(m_i r_{i_z})} \tag{2}$$

$$x_{ZMP} = \frac{\sum_{i=1}^{n}(r_{i_x}m_i a_{i_z} - r_{i_z}m_i a_{i_x} - \dot{H}_{i_y}}{\sum_{i=1}^{n}(m_i r_{i_z})} \tag{3}$$

$$z_{ZMP} = 0 \tag{4}$$

where for each link i: m_i is the mass, r_i is the position vector of the COG, a_i is the acceleration of the COG and $\dot{H}_i$ is the torque. The subscripts x, y, z represent the components in their respective each direction. Here the links represent the moving components of the FLV: including the main body of the FLV, the mast and forks, and the payload. We must note that it may not be practical to measure the dynamics of the mast and payload on a FLV due to the construction of the FLV and risk of damaging the sensors.

Equations (2)-(4) show coupling between a, v, ω, $\dot{\omega}$, defined by the kinematics in equation (1), with the centripetal components represented by $\dot{H}$, and the dynamic balance.

This formulation of the ZMP assumes planar motion. This assumption may be used if we consider many FLVs experience only planar surfaces such as in a warehouse environment, or freight distribution centre.

3 Dynamic Balance Margin

The dynamic balance margin describes, using a scalar value, the toppling propensity. A value of 1 describes the most balanced position, whereas a value of 0 describes toppling. The measure proposed uses the Zero Moment Point and a barycentric coordinate system to calculate the measure.

The barycentric coordinate system can be used to describe a convex polygon with n vertices, where the system may be described by the coordinates

$$\boldsymbol{\lambda} = \{\lambda_1, \lambda_2, ..., \lambda_n\}$$

The coordinate system is characterised by three properties [Floater *et al.*, 2006]:

Property 1. $\boldsymbol{p} = \sum_{i=1}^{n} p_i \lambda_i$

Property 2. $\sum_{i=1}^{n} \boldsymbol{\lambda} = 1$

Property 3. $0 < \lambda_i \leq 1,\ i = 1, 2, .., n$

where the set of vertices $\boldsymbol{p}$ consists of vertices $p_1, p_2, ..., p_n$.

The centroid is where $\lambda_i = \frac{1}{n}$, $\forall i$. The coordinate λ_i is 0 when the point lies on the vertex and 1 at the opposite end of the polygon.

Using properties 1 and 2, we can devise a dynamic balance margin Ξ for an n vertex polygon, normalised by the coordinates of the centroid, where the coordinate $\boldsymbol{\lambda}$ corresponds to the ZMP mapped to barycentric coordinates

Property 3 and a normalising constant ensures $\Xi \in (0, 1]$ with 1 corresponding to the centroid and most balanced state and 0 to the degenerate ZMP.

For the case of the FLV we may use the following definition:

$$\Xi = An \min \boldsymbol{\lambda} \tag{5}$$

where n, the number of vertices, is the normalising constant and

$$A = \begin{cases} -1 & : \exists i \ \lambda_i < 0 \\ 1 & : otherwise \end{cases}$$

This definition has triangular contours with one continuous minima along the polygon edges as shown in Figure 3.

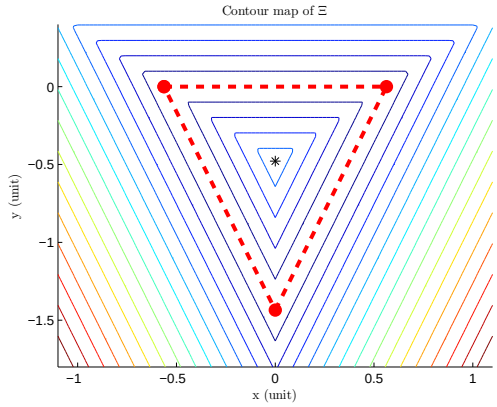

Figure 3: Contour map for Ξ. The dotted line represents the polygon, where $\Xi = 0$ with Ξ increasing away from $\Xi = 0$.

4 Dubins' and SCC path

The following subsections describe two geometric paths that have been used for non-holonomic motion planning. These paths will form the basis of our proposed path in Section 5.

4.1 Dubins' path

The Dubins' path describes the shortest distance between two poses, assuming there is no obstacle in between and a minimum turning radius that may be achieved instantaneously. The path consists of circular arcs and straight segments. The circular arc is defined by a maximum curvature κ_{max} which corresponds to the maximum curvature achievable by the vehicle. The premise of this path is to combine segments consisting of the components **L**, **R**, and **S**, where these letters represent left, right, and straight segments respectively, into words. Dubin [1957] found that the optimal distance path can be found using one of six words: LSR, LSL, RSR, RSL, RLR, and LRL. For brevity we may use C to represent the options L and R, condensing the six words into two forms: CSC, CCC. LaVille [2006] describes a Dubins' car to approximate a non-holonomic path; however the path itself is only G^1. The path is constructed with the assumption of unit or zero velocity.

4.2 Simple Continuous Curvature (SCC) path

The SCC path [Scheuer and Fraichard, 1997] builds on the Dubins' path to construct paths of G^2 continuity. Achieving G^2 continuity allows the trajectory to be C^2 continuous and hence non-holonomic. The SCC path attempts to reach κ_{max} for all turns unless the conditions for an elementary path is met [Scheuer and Fraichard, 1996]. The C element of the Dubins' path is replaced by what is known as a continuous curvature (CC) turn [Scheuer and Fraichard, 1997]. The CC turn consists of two symmetric clothoids [Scheuer and Fraichard, 1997], with a curvature $\kappa_i \leq \kappa_{max}$ and a circular arc of curvature κ_{max}. If an elementary path is used, the end pose of the CC turn remains the same as if the elementary path were not used. Similarly with the Dubins' path, the SCC path is constructed assuming unit or zero velocity.

The SCC can no longer claim distance optimality from the Dubins' path due to the change in the operational space from G^1 to G^2 continuity. Degtiariova-Kostova and Kostov [1998] finds the optimal solution for non-holonomic vehicles given finite turning rates may require an infinite number of switching points. This indicates that the optimal path may be arbitrary, without any describable form as the SCC solution attempts. The benefit of the SCC path is then not the optimality but the reduced search space.

The SCC path does not account for changes in behaviour due to changes in state. This is acceptable when the likelihood of toppling is low, as in common automotive vehicles. However, in the case of an FLV, small changes in acceleration and velocity may result in toppling, this is more pronounced when a heavy load is held high.

5 Modified SCC (mSCC) Path

Integration of the dynamics into a trajectory planner allows construction of a trajectory that abides by the dynamic constraints. In general, FLVs are non-holonomic vehicles, hence require a non-holonomic, or C^2 continuous, trajectory. To achieve a non-holonomic trajectory the following necessary condition is required for the geometry of the path:

$$G^2 \Rightarrow C^2$$

We propose a geometric trajectory planner that is both G^2 continuous and considers time dependent components in conjunction with constraints based on a dy-

namic balance margin. The trajectory planner will extend the existing SCC path to consider time varying parameters, resulting in a less conservative path. The planner will be further constrained by the dynamic balance margin, which will utilise the ZMP and a barycentric coordinate system to define the dynamic balance constraint.

This paper proposes the following changes to the construction of the SCC path to account for both the velocity in path construction and the dynamics:

1. Allow the two turns to have different curvatures κ_1, κ_2
2. Relax the requirement of reaching κ_{max}
$$\kappa_i \leq \kappa_{max}$$
3. Introduce non-unit time in the turning rate σ
$$\sigma_{eff} = \frac{\sigma_{max}}{v}$$
4. Use an optimisation process to choose the velocity on the interior points $\boldsymbol{v}$ of the path, and κ_1, κ_2.

If an SCC path is designed to prevent toppling then the CC turns will be designed for the worst case of the two turns, leaving the other turn to be highly conservative. The first modification relaxes the necessity for the turns to be the same, removing this issue.

The second modification models a real vehicle more accurately, where reaching the maximum curvature is not the goal. The SCC path provides one possible solution for this in the form of elementary paths. The use of $\kappa < \kappa_{max}$ provides a larger set of solutions that may solve the same issue as the elementary path.

One deficiency of both the Dubins' and SCC path is the lack of consideration of velocities in the construction of the path. The CC turns contains the velocity dependent components. The velocity dependent components are divided into two parameters: κ and the turning rate σ. κ has been addressed by modifications 1 and 2, leaving σ to be addressed. By introducing $\sigma_{eff}(v)$ the distance required to achieve a turn is changed. One mode of operation found in FLVs, is the ability to rotate on the spot, in this case velocity of the body is reduced to 0, $\sigma_{eff} = \infty$ and $\kappa_{max} = \infty$, allowing any heading to be reached within 0 distance.

To resolve these additions, which add to the problem search space, additional optimisation steps are required. The parameters to be optimised are the set of velocities that define the start and ends of each segment and the curvatures of the two turns, with the cost Q.

$$Q^* = \arg\min_{Q} w_s \frac{s(\boldsymbol{v}, \sigma_{max}, \kappa_1, \kappa_2)}{s_{nom}} + w_t \frac{t(q_s, q_f, \mathbf{v})}{t_{nom}} \tag{6}$$

The cost function (6) minimises the sum of the distance $s(\cdot)$ and time to travel $t(\cdot)$ normalised by the Euclidean distance between the initial and final poses s_{nom}. Note that $t(\cdot)$ is normalised by the time taken to travel t_{nom}, where $t_{nom} = s_{nom}$ given unit velocity. Ξ is a hard constraint on the optimisation preventing unsafe trajectories due to the single continuous global minima. The distance and time metrics are weighted by w_s and w_t respectively.

With the chosen $\boldsymbol{v}$, a continuous acceleration profile is used to interpolate between the velocities, to form a C^2 continuous trajectory. The choice of acceleration is left omitted to allow flexibility of controller choice.

To demonstrate the applicability of the mSCC path for FLVs, an illustration will be provided in the following section.

6 Computational Illustration

This section will be split into two illustrations. The first illustration will present a brief comparison between the mSCC trajectory and the Dubins' and SCC paths. There are, however, issues with a direct comparison, which will be explained further in 6.1.

Section 6.2 will compare common loading scenarios using a miniature FLV as a model. The miniature FLV will be used in future work experimentally verify the computational simulations, before use on real FLVs. Five cases will be illustrated in this section. Case 1-4 cover common loading scenarios, varying the height h and eccentricity of the load e. Case 5 explores a capability of the trajectory presented in this paper. Table 3 summarises the Cases 1-5. It must be noted that the cases presented are exaggerations, using a situation that pushes the limit of the models capability. For brevity all distances are measured in meters while time is in seconds.

6.1 Comparison of mSCC

This section compares the two Dubins' class paths presented in Section 4 to the mSCC trajectory but will first explain the deficiencies in a direct comparison. As previously mentioned, the three paths are not directly comparable due to the differences in assumptions. The change in difference in continuity assumptions effect either how the vehicle tracks the trajectory, assuming the vehicle may not be changed. Table 1 summarises the differences. We note that the comparison is useful to demonstrate graphically the differences in the three methods.

Perhaps the most immediate of problems regarding the comparison is the different velocity domains. The unit velocity assumption undermines the dynamic constraint formulation, where Ξ cannot be calculated when the paths are constructed. This problem further extends to the turning rate. The reliance on $\mathbf{v}$ for the mSCC trajectory results in transitional clothoids of different

Property		Dubins'	SCC	mSCC
Min. Continuity		G^1	G^2	G^2
Turning rate	σ	∞	$\sigma_{\max}$	$f(\sigma_{\max}, \mathbf{v}(\mathbf{t}))$
Velocity	$\mathbf{v}$	[0,1]	[0,1]	$[v_{\min}, v_{\max}]$

Table 1: Assumptions that directly effect suitability of comparisons. Note that the effects of each property is coupled.

lengths. Low velocities cause shorter transitions, while high velocities result in long transitions. Therefore different terminal velocities change only the mSCC path. The SCC and Dubins' path will handle the change in terminal velocities by either deviating from the path or reducing velocities to achieve the dynamic constraints.

The Dubins' path, specifically, has a number of problems when comparing to the mSCC trajectory. The minimum G^1 continuity and, similarly, $\sigma \to \infty$ results in the dynamic constraints breaking down. The result is the rotational accelerations tend to infinity causing $\Xi \to \infty$. Again this results in the inability to calculate Ξ directly.

In light of these issues we shall not attempt to conclude any quantitative difference and, as such, the parameters used for the model are unimportant and will be omitted for brevity and will state the model is based on the Hyster R1.4 Reach Truck shown in Figure 1.

The comparison in Figure 4 assumes the curvatures of the Dubins' and SCC paths are equivalent and lie on the boundary of operation. Terminal configurations q_s and q_f are fixed for all approaches. The FLV accelerates form an initial velocity $v_s = 0.5$ m/s to a final velocity $v_f = 3$ m/s. The resulting Dubins' path is shorter than the other approaches at $s_d = 28.44$, while the SCC travels $s_{SCC} = 34.84$ and the mSCC $s_{mSCC} = 33.67$. The mSCC path exhibits a tighter first turn $\kappa_1 < \kappa_2$. This, coupled with a appropriately small σ results in a shorter path than the SCC path. Again, we note that the mSCC trajectory may not be strictly shorter than the SCC path if velocities are greater.

A quantitative comparison of the three approaches is of little consequence to the purpose of the mSCC path, where the added domain of time is of more importance. This time variability allows distinction between states during the construction of the trajectory. The distinction in states can be observed in the following section.

6.2 Loading Scenarios

This section provides insight into the mSCC trajectory and common loading scenarios. The scenarios presented are exaggerated to better illustrate the behaviour the mSCC trajectory.

The model used in the following scenarios is a three wheeled miniature FLV. This miniature FLV will be used in the future to experimentally verify the approach before use on a real FLV. The miniature FLV resembles the Hyster R1.4 Reach Truck used in Section 6.1. The dimensions of the miniature FLV are summarised in Table 2. Since the CoG of the load is varied, we denote h and e as the height and eccentricity of the load CoG. The mass of the load $m_l = 4$ kg will be used for all scenarios excluding the unloaded scenario.

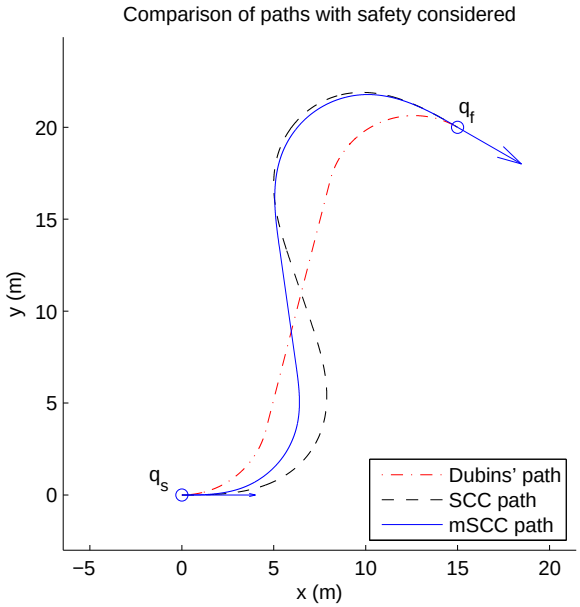

Figure 4: Comparison of Dubins', SCC and mSCC paths. $s_d = 28.44$ m, $s_{SCC} = 34.84$ m, $s_{mSCC} = 33.67$ m.

Parameter		Value	
wheelbase	d	0.5	m
track	t	0.6	m
mass of FLV		8	kg
distance weight	w_s	1	
time weight	w_t	1	
CoG		$[-0.29, 0, 0.18]^T$	m
CoG of load		$[0.2, e, h]^T$	m

Table 2: Parameters used in the simulation. The parameters are modelled after a R1.4 Reach Truck. h is the height of the load, while e is the eccentricity.

The five cases presented are summarised in Table 3. The scenarios will begin with an initial velocity of 2 m/s and arrive at a final velocity of 4 m/s. The terminal configurations used are the same for all scenarios. For ease of interpretation we will use radius of curvature $r_i = 1/k_i$ in place curvature.

Case 1: Unloaded FLV

Case 1, shown in Figure 6, presents a base case for Cases 2 and 3 to be compared. Here we see the FLV turn away

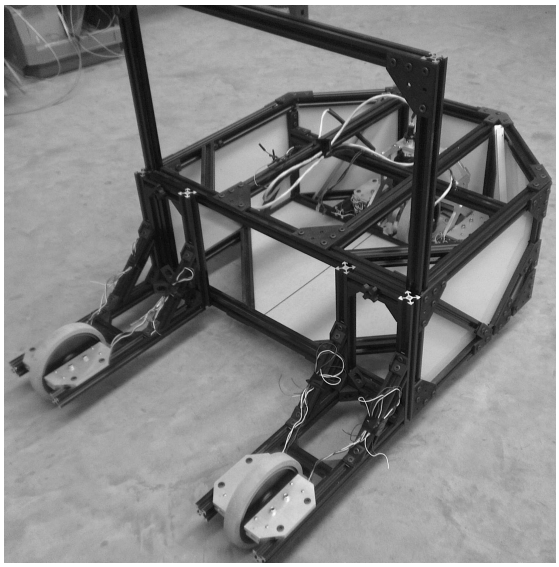

Figure 5: Miniature FLV currently under construction.

Case	h	e	m_l
1	0.0	0.0	0.00
2	0.6	0.0	4.00
3	1.2	0.0	4.00
4	1.2	0.2	4.00
5	On the spot turn		

Table 3: Different loading scenarios are addressed in cases 1-4, while case 5 presents a trajectory capable by the mSCC trajectory.

from the final pose, taking a sharper turn first before a much more gentle turn with radius of curvatures $r_1 = 1.50$ and $r_2 = 8.11$. The total distance travelled is $s_u = 19.96$ while the total time taken is $t_u = 6.51$.

The larger radius of curvature for the second turn is a result of the higher velocity required for q_f. The larger turning radius compensates for the increased lateral forces from high speeds. We also note the non-direct path taken is caused by choosing such a large turning radius.

Case 2: Raised Load

Case 2 loads the model FLV with approximately half the weight of the model. The load is raised by approximately three times the height of the FLV CoG, to 0.6. The resulting path is shorter with the distance travelled $s_r = 19.02$. The added load results in tighter turning radii $r_1 = 1.24$ and $r_2 = 7.90$.

Comparing the turning radii, we observe the additional mass has improved the turning capabilities of the model. In this case the CoG has been shifted forward toward the larger lateral cross section of the triangular

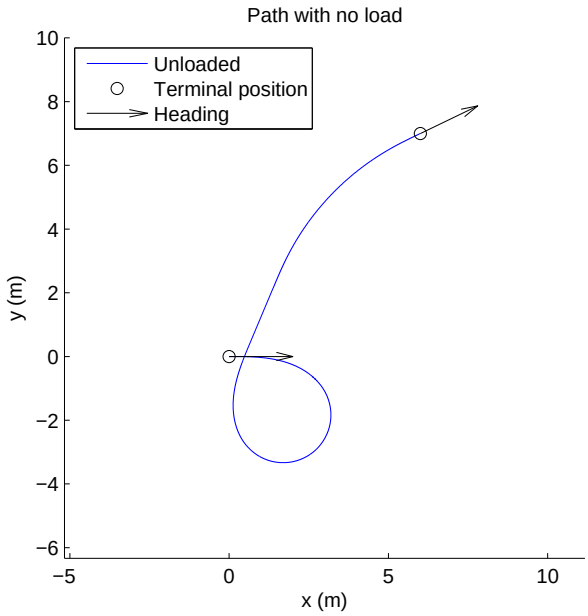

Figure 6: Trajectory with no load. $s_u = 19.96$, $r_1 = 1.50$, $r_2 = 8.11$, $t_u = 6.51$. Units in meters and seconds.

base. This is a common property of FLVs, where the counterbalance causes the FLV to be less balanced without a load than when a load is carried at low heights.

Case 3: High Load

Although Case 2 had a raised load, the performance was improved. Here we increase the load height by two fold, to $h = 1.2$, and observe a degradation in performance. Figure 8 compares Case 1 to Case 3. The second turn has a much larger turning radii than in Case 2 with $r_1 = 2.02$ and $r_2 = 22.50$, resulting in a distinct large circular motion to reach q_f. The total distance travelled is $s_h = 90.68$ with a time of $t_h = 40.23$.

After lifting the load past some height the performance begins to degrade, making toppling much easier. To account for this, the generated trajectory forces a much longer path to be taken, to both achieve the desired velocity and prevent toppling.

Case 4: High and Eccentric Load

Case 4 compares a high load with a high and eccentric load, shown in Figure 9. The same height is used here as in Case 3, with the load center shifted to the left of the vehicle by $e = 0.2$. This eccentricity results in the use of only left turns of radii $r_1 = 1.54$ and $r_2 = 11.34$. The new path is significantly shorter and faster than Case 3 with distance $s_e = 9.68$ and time $t_e = 23.71$.

The eccentric load causes atypical behaviour, allowing better turning in the direction that the load is laterally

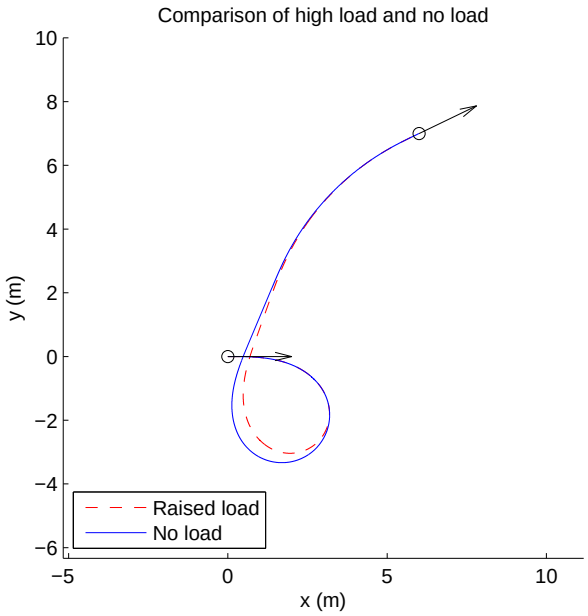

Figure 7: Comparison of Case 2 and Case 1. $s_r = 19.02$, $r_1 = 1.24$, $r_2 = 7.90$, $t_r = 6.15$. Units in meters and seconds.

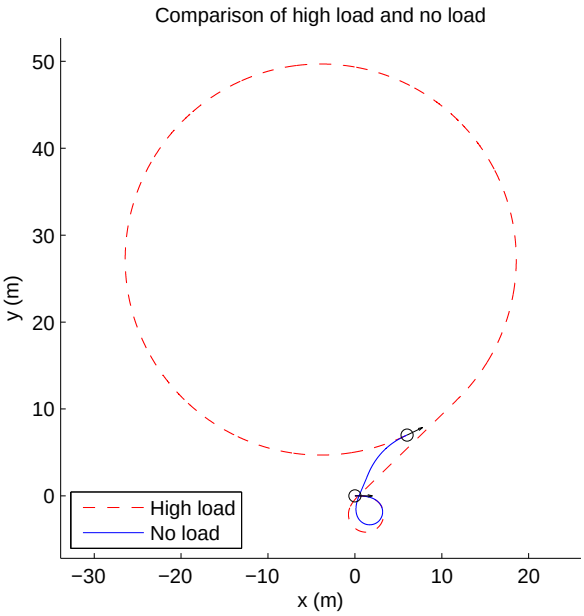

Figure 8: Comparison of Case 3 and Case 1. $s_h = 163.50$, $r_1 = 2.02$, $r_2 = 22.50$, $t_h = 40.23$. Units in meters and seconds.

offset. The loop observed in the first turn is used to increase the speed of the vehicle by increasing the distance travelled.

Case 5: Stationary Turn

The new mSCC path allows for FLV specific manoeuvres, specifically where the FLV may turn on the spot if the steering angle $\alpha = \pm\pi/2$, resulting in no translational motion, using equation (1), of point O as demonstrated in Figure 10. In this case $\sigma_{eff} \to \infty$ and $\kappa \to 0$ then the FLV may turn on the spot before continuing. However, this is not a condition one would impose on the general motion of the FLV, as it would require the vehicle to frequently stop. In a practical application, this is particularly useful when the vehicle is in a confined or narrow space, such as an aisle or loading area. The scenario where an FLV has just retrieved a payload from an aisle and is ready to move to the next destination illustrates this case.

7 Future Work and Conclusion

In this paper, we have proposed a trajectory planner incorporating dynamic balance and velocity into a geometric type path planner to achieve safe motion of a FLV. The new planner allows on the spot rotations and consideration of changing states to achieve a less conservative path than otherwise would occur with the SCC path. The new path also makes considerations toward the dynamic balance of the vehicle, using the ZMP to handle the coupling of parameters in relation to the dynamic balance. This novel dynamic balance margin is suitable for gradient based constraints used in optimisations due to the single continuous minima.

The new planner does not aim to be the optimal distance path, or time path, but make use of geometric properties to reduce the problem search space; hence requiring lower computational resources for use in the industrial setting. For this purpose, we accept the sub-optimality of such a scheme.

The computational illustrations provide an insight into typical scenarios, albeit exaggerated. Knowledge of FLV dynamic behaviour can be utilised for motion planning strategies in future work.

The miniature FLV, Figure 5, used in the computational illustrations will be used to test on hardware the trajectory generator presented in this paper, before being tested on a R1.4 Reach Truck shown in Figure 1.

Acknowledgments

This research was supported under Australian Research Council's *Linkage Projects* funding scheme (project number LP130100113) in collaboration with Speedshield Technologies Australia.

References

[Degtiariova-Kostova and Kostov, 1998] E Degtiariova-Kostova and V Kostov. Irregularity of optimal trajec-

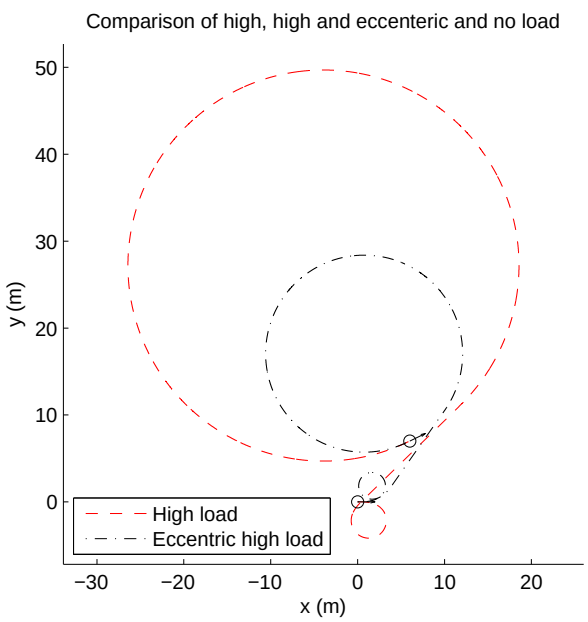

Figure 9: Comparison of Case 3 and Case 4. $s_e = 90.68$, $r_1 = 1.54$, $r_2 = 11.34$, $t_e = 23.71$. Units in meters and seconds.

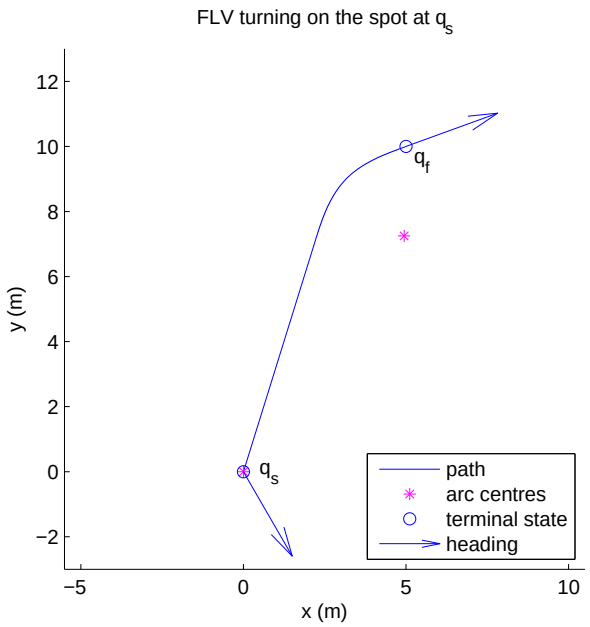

Figure 10: mSCC path allowing on the spot turns when $v = 0$.

tories in a control problem for a car-like robot. *Rapport de recherche INRIA*, (3411), 1998.

[Dubins, 1957] L E Dubins. On curves of minimal length with a constraint on average curvature, and with prescribed initial and terminal positions and tangents. *American Journal of Mathematics*, (3):497, 1957.

[Floater *et al.*, 2006] M S Floater, K Hormann, and G Kós. A general construction of barycentric coordinates over convex polygons. *Advances in Computational Mathematics*, 24(1-4):311 – 331, 2006.

[Gagliardi *et al.*, 2012] J-P Gagliardi, J Renaud, and A Ruiz. Models for automated storage and retrieval systems: a literature review. *International Journal of Production Research*, 50(24):7110 – 7125, 2012.

[Girbés *et al.*, 2014] V Girbés, L Armesto, and J Tornero. Path following hybrid control for vehicle stability applied to industrial forklifts. *Robotics and Automation Systems*, 62(6):910 – 922, 2014.

[Horberry *et al.*, 2004] T Horberry, T J Larsson, I Johnston, and J Lambert. Forklift safety, traffic engineering and intelligent transport systems: a case study. *Applied Ergonomics*, 35(6):575 – 581, 2004.

[Lapapong and Brennan, 2010] S Lapapong and S N Brennan. Terrain-aware rollover prediction for ground vehicles using the zero-moment point method. *American Control Conference (ACC), 2010*, page 1501, 2010.

[Larsson and Rechnitzer, 1994] TJ Larsson and G Rechnitzer. Forklift trucks-analysis of severe and fatal occupational injuries, critical incidents and priorities for prevention. *Safety Science*, 17(4):275 – 289, 1994.

[LaValle, 2006] S M LaValle. *Planning algorithms*. Cambridge university press, 2006.

[Popescu and Nastase, 2012] S Popescu and C Nastase, S Csatlos. Contributions to theoretical and experimental study of the dynamic stability of the forkfork trucks. *Journal of Engineering Studies and Research*, (3):115, 2012.

[Scheuer and Fraichard, 1996] A Scheuer and T Fraichard. Planning continuous-curvature paths for car-like robots. In *Procs. IEEE/RSJ International Conf. on Intelligent Robots and Systems*, volume 3, pages 1304–1311 vol.3, Nov 1996.

[Scheuer and Fraichard, 1997] A Scheuer and T Fraichard. Continuous-curvature path planning for car-like vehicles. In *Procs. IEEE/RSJ International Conf. on Intelligent Robots and Systems*, volume 2, pages 997–1003 vol.2, Sep 1997.

[Victorian WorkCover Authority, 2012] Victorian WorkCover Authority. Safety and prevention - forklifts, http://www.vwa.vic.gov.au/safety-and-prevention/health-and-safety-topics/forklifts, 2012.

[Vukobratović and Borovac, 2004] M Vukobratović and B Borovac. Zero-moment point - thirty five years of

its life. *International Journal of Humanoid Robotics*, 1(1):157, 2004.

[Vukobratović and Juricic, 1969] Miomir Vukobratović and Davor Juricic. Contribution to the synthesis of biped gait. *IEEE Transactions on Biomedical Engineering*, 16(1):1–6, 1969.

[Vukobratović *et al.*, 2006] M Vukobratović, B Borovac, and V Potkonjak. ZMP - A review of some basic misunderstandings. *International Journal of Humanoid Robotics*, 3(2):153 – 175, 2006.